

Robust Data Preprocessing for Machine-Learning-Based Disk Failure Prediction in Cloud Production Environments

Shujie Han[†], Jun Wu[‡], Erci Xu[‡], Cheng He[‡], Patrick P. C. Lee[†],
Yi Qiang[‡], Qixing Zheng[‡], Tao Huang[‡], Zixi Huang[‡], Rui Li[‡]
[†]The Chinese University of Hong Kong [‡]Alibaba

Abstract—To provide proactive fault tolerance for modern cloud data centers, extensive studies have proposed machine learning (ML) approaches to predict imminent disk failures for early remedy and evaluated their approaches directly on public datasets (e.g., Backblaze SMART logs). However, in real-world production environments, the data quality is imperfect (e.g., inaccurate labeling, missing data samples, and complex failure types), thereby degrading the prediction accuracy. We present RODMAN, a robust data preprocessing pipeline that refines data samples before feeding them into ML models. We start with a large-scale trace-driven study of over three million disks from Alibaba Cloud’s data centers, and motivate the practical challenges in ML-based disk failure prediction. We then design RODMAN with three data preprocessing techniques, namely failure-type filtering, spline-based data filling, and automated pre-failure backtracking, that are applicable for general ML models. Evaluation on both the Alibaba and Backblaze datasets shows that RODMAN improves the prediction accuracy compared to without data preprocessing under various settings.

I. INTRODUCTION

Modern cloud data centers are equipped with millions of hard disk drives spanning across the globe [1], [39]. With such a million-scale fleet of disks, disk failures become prevalent, complex, and cascading. For a data center equipped with high-end disks with an annual failure rate of 1% [35], administrators need to handle hundreds of disk failures/replacements on a daily basis. While data centers in practice are protected by RAID or erasure coding for fault tolerance, frequent disk failures or concurrent disk failures in a single disk group still lead to data unavailability [27]. To maintain data availability, it is crucial for administrators to be not only reactive to disk failures that have occurred, but also *proactive* to imminent disk failures, in large-scale disk deployment.

Recent studies show that machine learning (ML) can accurately predict imminent disk failures based on the already available SMART (Self-Monitoring, Analysis and Reporting Technology) logs in modern disks [10], [19], [24], [25], [28], [38]–[40], [42]. At a high level, existing ML-based disk failure prediction approaches first build a classifier model using the features (e.g., SMART attributes) of a training dataset that labels both positive and negative samples (i.e., failed and healthy disks, respectively). They then predict if a disk will fail within days or weeks by feeding its features into the classifier model. Despite the extensive studies in the literature, applying ML to disk failure prediction still faces three practical challenges in a complex cloud production environment.

(i) *Inaccurate labeling.* Existing studies often label fail-stop events as the only positive samples [10], [28], [39]. However, field studies report that soon-to-fail disks experience latent anomalies prior to actual failures, such as latent sector errors [9] and fail-slow symptoms [18]. Such pre-failure anomalies should also be labeled as positive samples, so as to reflect more accurately the failure patterns. To include pre-failure anomalies, a naïve solution is that during the training phase, we label the samples as positive if they appear within some pre-failure period before the actual failures occur. However, such a solution has two issues. First, it is unclear how to configure the “right” length of the pre-failure period without holistic measurements. Second, the pre-failure status of a failed disk is determined only after its failure actually occurs. If the failure event occurs right after the training phase, the samples before the failure event remain to be marked as healthy (negative), which still inaccurately reflects the failure status of those samples.

(ii) *Incomplete datasets.* Disk failure prediction becomes inaccurate if it operates on incomplete SMART logs; for example, field studies report that more than half of SMART failure signals are missing in failed disks [32]. In production, disk monitoring systems may stop recording failure signals due to network failures, software maintenance/upgrades, system crashes, and human mistakes [17]. In our production experience, some special commercial activities may require the suspension of the disk monitoring systems for server offloading. One solution is to interpolate the missing failure signals, but improper interpolation can severely compromise the prediction accuracy.

(iii) *Diverse failure types.* Disk failures can manifest in different forms, such as disk crashes, or fine-grained errors like latent sector errors [9], [34] and data corruptions [8]. Some failures are due to accumulated factors such as frequent occurrences of sector errors [34], while others are due to transient factors such as power faults [41] or faulty interconnects [21]. SMART logs provide insufficient details to address the diverse types of disk failures.

We present RODMAN, a robust disk failure prediction management pipeline designed to address the above three challenges. Our goal is to emphasize the necessity of proper preprocessing on the training datasets when deploying disk failure prediction in the field. Note that some existing ML-based disk failure prediction approaches (e.g., [10], [28], [38]) are directly evaluated on the public Backblaze SMART logs [3]. However, we find that the Backblaze dataset also shares the

above three challenges (i.e., only fail-stop events are labeled as positive samples, data missing exists, and failure types are unavailable). Such approaches, when re-evaluated under different deployment settings, give inaccurate prediction if the training datasets are not properly preprocessed.

RODMAN uses three data preprocessing techniques to refine data samples from a large-scale dataset before feeding them into ML model training. Its techniques are applicable for general ML models. RODMAN is now deployed in the production data centers at Alibaba Cloud. We summarize our contributions as follows.

- We conduct a measurement study on a one-year span of disk logs from a fleet of more than three million disks deployed at Alibaba Cloud, so as to motivate the need of data preprocessing in practical disk failure prediction. To our knowledge, our measurement study is among the largest scale in the literature. See §II and §III.
- We propose three data preprocessing techniques, namely: (i) *failure-type filtering*, which selects only the positive samples of statistically predictable failure types for training; (ii) *spline-based data filling*, which fills the values of missing samples via cubic spline interpolation [37] to account for any possible abrupt changes in such missing samples; and (iii) *automated pre-failure backtracking*, which not only automatically determines a window of pre-failure samples that are to be labeled as positive for any soon-to-fail disk, but also avoids mis-labeling any failed disk that appears right after the training phase. See §IV.
- We evaluate the accuracy gain of each data preprocessing technique on both Alibaba and Backblaze datasets. RODMAN achieves a disk failure prediction rate of up to 92.8% and 82.4% under a false positive rate of 0.1% and 4.0% on the Alibaba and Backblaze datasets, respectively, and improves the accuracy by 6.2-23.7% over state-of-the-art ML-based disk failure prediction approaches [10], [28]. See §V.

II. METHODOLOGY

We collect data from a production cloud infrastructure at Alibaba Cloud that covers multiple data centers across the globe. Each data center is composed of multiple nodes organized in racks, and each node is attached with multiple disks.

Figure 1 depicts our data collection architecture. We collect three types of data: *SMART logs*, *system logs (syslogs)*, and *trouble tickets* (see details below). Each node collects SMART logs from its attached disks and syslogs from its operating system, and periodically reports the collected data to one of the proxies of our data collection architecture. The proxies relay the collected data to a data processing service, called MaxCompute [5] that supports an SQL-like interface for users to query the stored data similar to Hive [2]. Also, we deploy a maintenance system that identifies abnormal disk behaviors and submits the corresponding trouble tickets to the data processing service. RODMAN takes the three types of data as input, performs data preprocessing, and predicts disk failures.

We refer to our collected dataset as the *Alibaba dataset*. It was collected over a one-year span from July 2017 to June

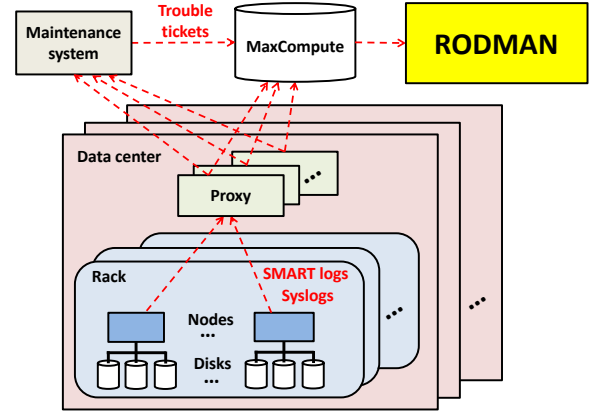


Figure 1: Overview of data collection.

2018. It covers a population of over three million disks of tens of disk models from five disk vendors, and the disks are deployed in dozens of data centers across the globe. Table I summarizes the dataset, which includes three types of data.

SMART logs. SMART is a widely used disk status reporting tool that collects performance and reliability statistics for different *attributes* at disk firmware. Our SMART logs cover the error-related or status-related attributes for all disks at different times. Each SMART log entry is a key-value pair, in which the key is the disk ID (serial number), and the value contains the disk model, disk vendor, timestamp, and a list of SMART attributes. Each attribute is a numerical value. It is either normalized (e.g., wearing percentage) or raw (e.g., power-on hours), and either instantaneous (e.g., temperature) or cumulative (e.g., number of reallocated sectors).

Our collected SMART attributes are vendor-specific and the number of collected attributes varies across different disk vendors. Nevertheless, we find that most disk models report at least 38 attributes. Also, all attributes related to disk errors are universally reported at the daily granularity. In our one-year span, our SMART logs cover over one billion entries.

Syslogs. All nodes in this study run the major Linux distributions. The Linux kernel is installed with the syslog daemon [16] that is configured to collect system-level events at the hourly granularity. Each syslog event contains the process ID, timestamp, and description of the event (e.g., the disk is not found). It also specifies the logical partition (e.g., /dev/sda) that allows us to automatically correlate each event with a disk. Syslog events can be categorized into different severity levels. We focus on five of them triggered by disk failures: Emergency, Alert, Critical, Error, and Warning. In our one-year span, our syslogs cover over four trillion entries.

Trouble tickets. Our maintenance system applies rule-based checking procedures defined by administrators to the SMART logs and syslogs, so as to check for any abnormal behaviors, including kernel-level errors/alerts and SMART error-related attributes that are above some pre-configured thresholds. For any abnormal behavior, the maintenance system generates a trouble ticket, which contains the node ID, disk ID, timestamp, and a description about the error (e.g., a snippet of the syslog

Source	Format	Description	Granularity	Total size
SMART logs	Key-value pairs	Disk status reports	Daily	> 1 billion log entries
Syslogs	Plain texts	Kernel runtime events	Hourly	> 4 trillion entries
Trouble tickets	Event entries	Node ID, disk ID, timestamp, and error messages	Per event	~31,000 events

Table I: Dataset overview.

event message). In our one-year span, we have collected around 31,000 trouble tickets.

III. DATA ANALYSIS

To motivate the design of RODMAN, we first analyze the Alibaba dataset, with emphasis on the disk failure patterns in production and the data missing issue in the dataset (§III-A). Due to privacy concerns, we cannot publicize the Alibaba dataset at the time of the writing. Thus, we also analyze the public Backblaze dataset [3] for cross-validation (§III-B).

A. Alibaba Dataset

Annualized failure rates. We first estimate the annualized failure rates (AFRs) of several representative disk models. We define the AFR as the ratio of the number of failed disks reported in our trouble tickets in the one-year span of our dataset to the total number of disks.

Recall that the Alibaba dataset covers tens of disk models from five disk vendors (§II). We focus on the three largest models with the most disks within each vendor (i.e., 15 in total). We denote each disk model by “Vendor” k , where “Vendor” corresponds to a letter (‘A’, ‘B’, ‘C’, ‘D’, and ‘E’) for each of the five vendors, and “ k ” (1 to 3) corresponds to the k -th numerous model; for example, the disk model “A2” represents the second numerous model of vendor A.

Table II presents the results of the 15 selected disk models. The AFR of each disk model is at most 3.8%, and most disk models (10 out of 15) have an AFR of less than 1%. Such low AFRs are also found in previous disk failure prediction studies [10], [39], and hence we must address the well-known *data imbalance* issue (i.e., the number of failed disks is much less than that of healthy disks).

Failure types. We now correlate both syslogs and trouble tickets to identify the manifested failure types in production. We classify the disk failures reported in trouble tickets into six major types, namely data corruptions, I/O request errors, unhandled errors, disk-not-found errors, unhealthy disks, and file system corruptions. We focus on the two largest disk models (in terms of the number of disks in our dataset), A1 and B1, as the representatives. Table III shows each failure type and the proportions of all failures in two disk models A1 and B1.

Data corruptions and I/O request errors are the most dominant failure types (44.1% and 19.1% for A1, and 39.2% and 45.5% for B1, respectively). Data corruptions refer to the unrecoverable data loss (e.g., integrity check errors) that cannot be directly detected by disks [8], while I/O request errors refer to the failed I/O requests (e.g., due to bad sectors or transient disconnection) that are detectable by disks.

Unhandled errors (18.4% and 9.8% for A1 and B1, respectively) occur when failed disks return unknown error codes after

Model	Vendor%	Total%	AFR
A1	27.7%	12.5%	0.56%
A2	21.1%	9.5%	0.67%
A3	18.2%	8.2%	0.59%
B1	29.2%	10.8%	0.68%
B2	28.1%	10.3%	0.64%
B3	20.1%	7.7%	0.38%
C1	30.1%	2.5%	3.8%
C2	18.6%	1.5%	2.8%
C3	11.0%	0.88%	1.1%
D1	41.6%	2.7%	0.30%
D2	25.1%	1.6%	1.0%
D3	18.9%	1.2%	2.0%
E1	62.9%	1.7%	0.53%
E2	14.6%	0.39%	0.78%
E3	13.5%	0.35%	0.65%

Table II: Failure patterns for different disk models in the Alibaba dataset, including the percentage of disks in the same vendor (“Vendor%”), the percentage of disks in the whole disk population (“Total%”), and the annualized failure rate (“AFR”). Due to privacy concerns, we cannot report the number of disks for each disk model.

Type	Description	A1	B1
Data corruptions	Unrecoverable data loss (e.g., integrity check errors)	44.1%	39.2%
I/O request errors	Failed I/O requests (e.g., bad sectors, transient disconnection)	19.1%	45.5%
Unhandled errors	Unknown disk error codes (e.g., unrecognized error codes, unexpected corruption to error codes)	18.4%	9.8%
Disk-not-found errors	Disk component failures (e.g., faulty interconnects)	6.8%	1.5%
Unhealthy disks	Soon-to-fail disks reported by rule-based checking	2.1%	Nil
File system corruptions	Unmountable file system (e.g., meta-data corruption)	Nil	0.19%
Others	No further information	9.1%	3.9%

Table III: Failure types for disk models A1 and B1.

receiving I/O requests from the kernel. For example, the kernel does not recognize an error code defined by the disk vendor, or failed disks encounter unexpected errors (e.g., on-chip memory corruption) that give meaningless error codes.

Disk-not-found errors (6.8% and 1.5% for A1 and B1, respectively) refer to the permanent disk component failures (e.g., faulty interconnects) that make the whole disks detached from the kernel. They differ from I/O request errors, in which the disks remain attached.

Unhealthy disks (2.1% for A1, but not found for B1) are reported by our internal rule-based checking tool based on SMART logs. The tool periodically checks several SMART attribute values against pre-specified thresholds, and reports the disks that likely fail soon (e.g., too many sector errors).

File system corruptions (0.19% for B1, but not found for A1) refer to the disks with unmountable file systems. They are a rare failure type, as modern file systems provide protection

Model	Failed			Healthy
	DMR	10 days%	25 days%	DMR
A1	21.1%	43.5%	31.7%	6.3%
A2	21.3%	33.6%	14.4%	6.6%
A3	22.4%	51.0%	36.7%	7.3%
B1	28.1%	23.4%	15.1%	6.8%
B2	29.5%	15.7%	13.4%	5.8%
B3	20.8%	16.2%	12.5%	8.4%
C1	15.4%	73.7%	36.8%	7.4%
C2	13.2%	36.8%	21.1%	6.1%
C3	18.5%	40.0%	40.0%	6.1%
D1	19.5%	33.3%	16.7%	6.0%
D2	13.2%	22.2%	33.3%	6.4%
D3	12.9%	50.0%	0%	6.1%
E1	16.7%	56.7%	56.7%	16.3%
E2	14.2%	0%	0%	15.6%
E3	14.6%	20.0%	20.0%	9.7%

Table IV: Data missing analysis for different disk models in the Alibaba dataset, including the data missing ratios (DMRs) for failed and healthy disks, as well as the percentages of data-missing failed disks that miss at least consecutive 10 and 25 days of samples before being reported in trouble tickets (“10 days%” and “25 days%”, respectively).

in metadata (e.g., error-correction codes in inode tables) [7].

Also, we cannot determine the failure types of small fractions of failed disks (9.1% and 3.9% for A1 and B1, respectively) due to the lack of recorded information.

Data missing. Ideally, the SMART data is collected for all disks continuously on a daily basis, yet our dataset contains incomplete SMART data in both failed and healthy disks (§I). Here, a disk is said to have data missing on a day if it misses *all* collected SMART attributes instead of some particular SMART attributes. To show the severity of data missing, we compute the *data missing ratio (DMR)* as the total number of missing days over the expected total number of occurrence days if no data missing occurs. For failed disks, we count the expected occurrence days from when the disks first appear in the dataset until they fail; for healthy disks, we only focus on those that appear at the beginning of the dataset, and hence the expected number of occurrence days is one year.

To examine the data missing behavior before a failed disk is reported in a trouble ticket, we measure the missing gap for any failed disk that has data missing between the last reported date of the SMART logs and the reported date of the trouble ticket. Here, we focus on the percentages of data-missing failed disks with such missing gaps of at least consecutive 10 and 25 days.

Table IV presents the results of our 15 selected disk models. Data missing of failed disks is more severe than that of healthy disks. For failed disks, the DMRs among 15 disk models are 12.9-29.5%, while for healthy disks, the DMRs are 5.8-16.3%. Also, the data-missing failed disks tend to miss data for a long consecutive period of days before being reported in trouble tickets. For example, 9 out of 15 disk models have at least 30% of data-missing failed disks with at least 10 days of data missing, while 8 out of 15 disk models have at least 20% of data-missing failed disks with at least 25 days of data missing, before the reported dates of trouble tickets.

To understand the pre-failure data missing issue, we study

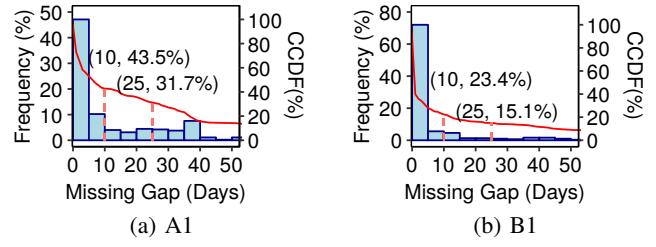


Figure 2: Missing gap distributions for data-missing failed disks in disk models A1 and B1.

Model	Failed			Healthy
	DMR	10 days%	25 days%	DMR
H1	0.31%	0%	0%	0.20%
S1	1.3%	0.08%	0.08%	0.36%

Table V: Data missing analysis for different disk models in the Backblaze dataset.

the distribution of the missing gap between the last recorded date of the SMART logs and the recorded date of the trouble ticket for a data-missing failed disk in the two largest disk models A1 and B1. Figure 2 shows the histograms and the complementary cumulative distribution functions (CCDFs) of the missing gap distributions for both disk models. Among the data-missing failed disks, 43.5% and 23.4% of data-missing failed disks in A1 and B1 have data missing for at least 10 consecutive days, respectively. This suggests that failed disks may have already exhibited abnormal behaviors before they are reported in trouble tickets, thereby leading to data missing.

B. Backblaze Dataset

We cross-validate our findings on the public Backblaze dataset [3]. We focus on two disk models that are used in prior studies [10], [28], [38] and have the largest population and the most failures: (i) Hitachi HDS722020ALA330 (denoted by H1) over a 18-month span from April 2014 to September 2015, and (ii) Seagate ST4000DM000 (denoted by S1) over a 40-month span from September 2014 to December 2017.

For H1, 133 out of 4,586 disks are failed, while for S1, 2,688 out of 32,320 disks are failed. The corresponding AFRs for H1 and S1 are 1.9% and 2.5%, respectively, similar to the AFRs in the Alibaba dataset. We find that data missing also exists in the Backblaze dataset (Table V), although the DMRs are much lower than those in the Alibaba dataset (Table IV). Unfortunately, the Backblaze dataset does not document the detailed failure symptoms or root causes, so we do not have failure-type details.

IV. RODMAN DESIGN

We present RODMAN, a robust disk failure prediction pipeline. Figure 3 shows RODMAN’s architecture. RODMAN takes the SMART logs, syslogs, and trouble tickets as input. It converts SMART logs into time-series samples, in daily granularity, for different disks. Each sample contains a set of SMART attributes at a time point. It uses syslogs and trouble tickets for failure-type correlation and labeling, respectively. It first refines the samples with three data preprocessing techniques that are

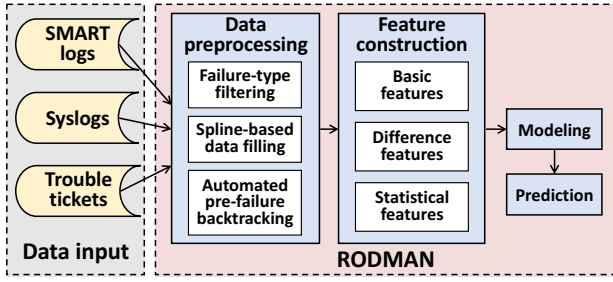


Figure 3: Architecture of RODMAN.

applied to training dataset before model training (§IV-A-§IV-C). It constructs features for model training (§IV-D). It finally performs modeling and outputs prediction results (§IV-E). We conclude this section with the implementation details of RODMAN (§IV-F).

Our analysis focuses on two largest disk models of the Alibaba dataset, A1 and B1, that have the most numbers of disks (and the most numbers of failed disks) among all disk models we consider. As they belong to different vendors, they are expected to have varying failure characteristics [8], [34]. We also validate our analysis for other disk models from both Alibaba and Backblaze datasets (§V). RODMAN focuses on offline learning and assumes that the whole training dataset is available in advance, while we address online learning on real-time data in future work.

A. Failure-Type Filtering

Recall from Table III that there are various types of disk-related failures. Our goal is to leverage the diverse failure types to help our model training in RODMAN.

Analysis. Before examining the failure type information, we first analyze the correlation between the SMART attributes and the disk failures reported by our trouble tickets. We compute Spearman’s Rank Correlation Coefficient (SRCC) [36] between each of the SMART attributes and disk failures. SRCC ranges from -1 to +1 and shows the positive/negative correlation between two variables; a larger absolute value (with the maximum equal to one) implies that the two variables are more correlated, while 0 means no correlation. In our case, one variable refers to the raw value of a SMART attribute, while another variable refers to the indicator variable whether a disk is failed (1 means failed, or 0 otherwise).

Table VI shows the four most failure-correlated SMART attributes for disk models A1 and B1 with the largest absolute SRCC values. Three of the SMART attributes appear in both A1 and B1, namely SM5 (Reallocated Sectors Count), SM197 (Current Pending Sector Count), and SM198 (Offline Uncorrectable Sector Count), and the remaining ones are SM187 (Reported Uncorrectable Errors) for A1 and SM196 (Reallocated Event Count) for B1. We find that no SMART attribute in either disk model is dominant, as the highest values are 0.401 and 0.352 for A1 and B1, respectively. Furthermore, Table VII shows the percentage of failed disks with zero values for the four most failure-correlated SMART attributes for A1

Model	SM5	SM187	SM197	SM198
A1	0.397	0.401	0.314	0.283
Model	SM5	SM196	SM197	SM198
B1	0.352	0.325	0.336	0.330

Table VI: Spearman’s Rank Correlation Coefficients of the selected SMART attributes and disk failures for A1 and B1.

Model	SM5	SM187	SM197	SM198	All
A1	49.6%	81.9%	60.8%	60.9%	43.9%
Model	SM5	SM196	SM197	SM198	All
B1	92.1%	92.1%	79.5%	94.0%	78.2%

Table VII: Percentage of failed disks with zero values in the selected SMART attributes for A1 and B1; “All” means that all four attributes have zero values.

Model	SMART	1	2	3	4	5	6	7
A1	SM5	✓		✓	✓	✓		✓
	SM187	✓				✓		✓
	SM197	✓				✓		✓
	SM198	✓			✓	✓		✓
B1	SM5	✓						
	SM196							
	SM197							✓
	SM198	✓						✓

Table VIII: KS test for evaluating the distribution differences of each SMART attribute between failed and healthy disks for A1 and B1, grouped by failure types (1: Data corruptions; 2: I/O request errors; 3: Unhandled errors; 4: Disk-not-found errors; 5: Unhealthy disks; 6: File system corruptions; 7: Others). A ✓ means that the distribution is statistically different.

and B1. We find that 43.9% and 78.2% of failed disks have zero values in all the four SMART attributes for A1 and B1, respectively, conforming to the prior study that many failed disks have zero values in failure-correlated SMART attributes [32]. Our results suggest that individual SMART attributes are weak indicators of disk failures.

Nevertheless, by grouping the SMART attributes by failure types, we can differentiate the distributions of SMART attribute values between the healthy and failed disks. Our insight is that only a subset of failures can be measured by SMART logs. If there is a larger discrepancy in the distributions, then the trained classifier can recognize such failures more easily. Specifically, we use the two-sample Kolmogorov-Smirnov (KS) test [29] to statistically evaluate the distribution discrepancies of each SMART attribute between the healthy and failed disks. Table VIII shows the KS test results, in which the statistically different distributions (with a confidence level of 95%) are marked with ticks (✓). We call a failure type *predictable* if there is more than one tick in the underlying SMART attribute distributions. Thus, the predictable failure types are data corruptions, disk-not-found errors, and unhealthy disks for A1, and data corruptions for B1.

We use the disk failures of predictable failure types to build our classifier; on the other hand, we filter any disk failure of unpredictable failure types. We do not consider training a different model for each failure type, as some failure types (e.g., unhealthy disks for A1 and file system corruptions for B1) have very limited positive samples for accurate training.

Our training procedure. We summarize our training pro-

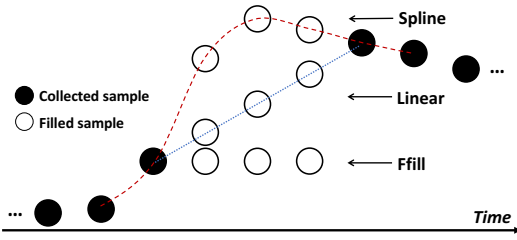


Figure 4: Comparison of interpolation approaches: forward filling (Ffill), linear interpolation (Linear), and cubic spline interpolation (Spline). Cubic spline interpolation provides better fitting for abrupt changes than other two approaches.

cedure based on failure-type filtering as follows. Before training a classifier for a particular disk model, we first choose a configurable number (four in our case) of most failure-correlated SMART attributes. We then parse the syslogs to group the failure types and compare the above SMART attribute distributions between the healthy and failed disks for different failure types with the KS test. Finally, we identify the failure types as predictable if there is more than one failure-correlated SMART attribute with statistically different distributions between the healthy and failed disks. When training the classifier, we only use the disk failures of predictable failure types as positive samples and discard the unpredictable ones.

B. Spline-based Data Filling

Before applying model training to a dataset, we must first address missing data samples in every failed or healthy disk. We discuss different data filling approaches.

Naïve data filling approaches. One naïve approach is *forward filling*, which fills any missing sample with the value of any last observed sample in the series (e.g., for the series “1, 2, miss, 3, 4”, we fill “miss” with “2”). Another naïve approach is *linear interpolation*, which fits any missing sample on a linear line that connects the endpoints of each missing gap (e.g., for the series “1, 2, miss, 3, 4”, we fill “miss” with “2.5”). Both approaches, albeit implementation-friendly, unfortunately cannot address complicated changes in SMART values. For example, the counts of error-related SMART attributes often ramp up abruptly for a soon-to-fail disk.

Our data filling approach. RODMAN uses *cubic spline interpolation* [37] to fill any missing samples. At a high level, for each missing gap over a time series, we select the two closest available data samples at both ends (i.e., four samples in total) to construct piecewise cubic polynomials that connect all four samples while ensuring a “smooth” polynomial. Cubic spline interpolation provides better fitting for the abrupt changes than the naïve approaches (see Figure 4 for comparisons), while avoiding oscillated fitting that occurs in high-degree polynomial interpolation (a.k.a. Runge’s phenomenon). It reduces to a linear function for the time series with stable monotonic trends (e.g., power-on-hours).

We address two corner cases in data filling. First, the missing gap may be open-ended, such that the missing samples may

be observed at the very beginning (or at the very end) of the dataset. In this case, we re-use the first (or the last) piecewise polynomial in the time series from our interpolation results to extrapolate those missing samples. Second, if the missing gap lasts longer than some pre-specified threshold (currently set to 30 days), we drop all the samples for the time series.

We do not claim that spline-based data filling can address the missing samples for all data types, yet it improves the prediction accuracy over naïve approaches (§V-B) and suffices for our practical deployment. Optimizing the data filling strategy is our future work.

C. Automated Pre-Failure Backtracking

To accurately reflect the disk failure characteristics, we propose to mark the pre-failure samples of failed disks as positive. However, the length of the pre-failure period is typically unknown. Thus, we need to address two questions: (i) How do we automatically determine the length of the pre-failure period? (ii) Given the pre-failure period, how do we properly backtrack and mark disk samples?

Automated determination of the pre-failure period. We identify the pre-failure period using *Bayesian change point detection* [15] for failed disks in SMART logs, so as to pinpoint the time when the SMART values of failed disks significantly vary (i.e., the failure behaviors start to appear). Specifically, during our training procedure for each disk model, we first identify the four most failure-correlated SMART attributes based on SRCC and select the failed disks of predictable failure types (§IV-A). We pick a sufficiently long detection window (e.g., 60 days in our implementation) before the failure happens for each failed disk that has already been labeled from trouble tickets. We compute the change probability (i.e., the posterior distribution of a time-series up to a sample given the time-series before the sample) of each of the four selected SMART attributes on each day for each failed disk over the detection window. Given a sequence of change probabilities over the detection window of each failed disk, we use the z-score (i.e., the number of standard deviations from the mean of change probabilities) to measure if the change is significant. We now choose the critical z-score values as ± 2.5 of the standard deviation (i.e., a confidence level of 98.76%), such that if the z-score of the change probability falls outside the range $[-2.5, 2.5]$, we regard the change as significant. We obtain the numbers of days between the significant change and the disk failure for all failed disks. Finally, we find the 75th-percentile of the numbers of days obtained for each of our selected failure-correlated SMART attributes, and choose the maximum 75-th percentile among the SMART attributes as our pre-failure period.

Based on our calculation, the pre-failure periods of A1 and B1 are 29 and 27 (days), respectively. Note that finding the pre-failure period can be automated, and the length of the pre-failure period varies for different disk models.

Pre-failure backtracking. Given the pre-failure period, we backtrack the pre-failure samples of a failed disk and mark

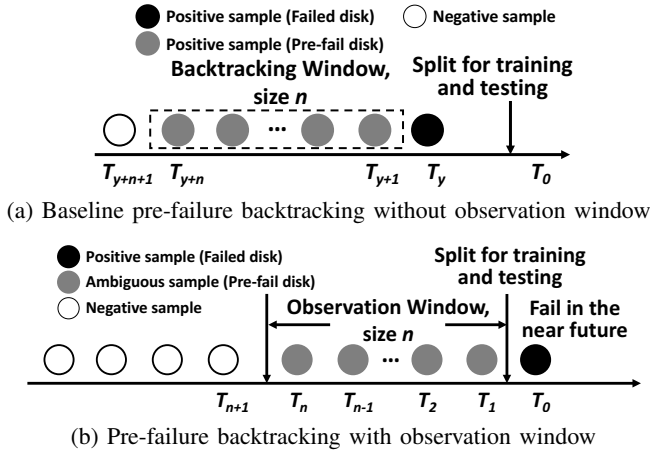


Figure 5: Pre-failure backtracking.

them as positive samples. We define a *backtracking window* as the number of backtracked days in which we mark the samples of a failed disk as positive. Currently, we set the backtracking window length (denoted by n) as the pre-failure period that is automatically selected for each disk model.

Figure 5(a) shows the *baseline* design of our pre-failure backtracking method. Suppose that the training phase is set right before day T_0 and the testing phase starts on day T_0 . Let T_i be the i -th backtracked day before T_0 at which a sample s_i is observed, where $i > 0$ (note that T_i is earlier than T_0). Let T_y (for some $y > 0$) be the last day on which the positive sample is observed (i.e., the disk failure occurs). Each dot in the figure represents a sample of SMART logs in daily granularity. We mark a failed disk at T_y as a positive sample (denoted by a black dot). We also mark n samples (denoted by gray dots) prior to the disk failure as positive samples. The earlier samples before the backtracking window are marked as negative samples (i.e., healthy) (denoted by white dots).

However, there exists a potential issue with the baseline pre-failure backtracking design. Recall that the maintenance system generates the trouble tickets of failed disks on the day of disk failure occurrence (§II). Thus, we regard the disks that are not reported in the trouble tickets as healthy in the training dataset, but the disks may fail right after the training phase and their samples now become “mis-labeled” as negative. Figure 5(b) illustrates the issue. If a disk fails right after T_0 (i.e., the black dot), then we are supposed to mark all samples of its backtracking window as positive samples (i.e., the gray points). However, we do not have this information during model training as the failure happens after the training phase. From this example, we see that for healthy disks, their samples in the backtracking window are actually ambiguous samples, as they may fail right after the training phase.

To avoid mislabeling negative samples, we propose an *observation window* to *drop* the ambiguous samples of pre-failure disks that are potentially mislabelled as negative. We now set the observation window as the backtracking window n and drop the (ambiguous) samples from T_n to T_1 .

Summary. Our complete pre-failure backtracking scheme with

the observation window works as follows. If a disk is healthy, we drop all its samples within the observation window (from T_n to T_1) and mark any sample outside the observation window (from T_{n+1} backwards) as negative. Otherwise, if a disk is failed (say in day T_y), we backtrack n samples within the backtracking window (i.e., from T_{y+n} to T_{y+1}) to mark them as positive, as well as the remaining samples outside the backtracking window as negative.

D. Feature Construction

Our feature construction uses three categories of features.

- **Basic features:** We select the error-related and status-related SMART attributes (§II) as the basic features.
- **Difference features:** For each SMART attribute selected as a basic feature, we calculate the difference values over two consecutive samples in the time-series.
- **Statistical features:** We compute six statistical characteristics for each basic/difference feature over a window of samples: arithmetic mean, standard deviation, median, exponential weighted moving average, sum, and difference between the start and end points of the window. We use two window sizes, 7 and 14 days, for computing the above statistical characteristics for each basic/difference feature.

For example, for A1 (B1), we obtain 1,248 (988) features, including 48 (38) basic features, 48 (38) difference features, and 1,152 (912) statistical features. Also, for H1 (S1) in the Backblaze dataset (§III-B), we obtain 884 (1,248) features, including 34 (48) basic features, 34 (48) difference features, and 816 (1,152) statistical features.

E. Modeling

We formulate our disk failure prediction problem as a time-series binary classification problem. Among many classification algorithms, researchers [12], [13] show that tree-based ensemble learning methods (e.g., random forests and boosted trees) have the best overall prediction accuracy. As RODMAN generates fewer than 4,000 features, it is shown that boosted trees are preferred [12], [13]. By default, RODMAN uses LightGBM [23], a boosted tree model with high training performance and memory efficiency, yet RODMAN is also applicable for other ML models (§V-C). Note that we do not claim the novelty of our modeling approach.

F. Implementation

We implement the whole RODMAN pipeline in Python with around 2,000 LoC. We use the authors’ Python implementation of LightGBM [4], and realize other ML algorithms for comparisons using various Python tools (e.g., NumPy [30], SciPy [22], and Scikit-learn [31]). RODMAN is currently deployed at Alibaba Cloud.

We also realize RODMAN for the Backblaze dataset. Since the Backblaze dataset does not include failure types, we only realize automated pre-failure backtracking and spline-based data filling. Our RODMAN prototype is now open-sourced (§I).

V. EXPERIMENTS

We evaluate RODMAN on both Alibaba and Backblaze datasets and show that its data preprocessing improves the prediction accuracy. We address the following questions:

- Can automated pre-failure backtracking identify the proper backtracking window length and improve the prediction accuracy? (Exp#1)
- Can failure-type filtering (i.e., using only predictable failure types for training) accurately predict disk failures of both predictable and unpredictable failure types? (Exp#2)
- How effective is spline-based data filling? (Exp#3)
- Can RODMAN improve the prediction accuracy over state-of-the-art disk failure prediction approaches? (Exp#4)
- How does the prediction accuracy of RODMAN vary for different configuration parameters (e.g., false positive rates and training periods)? (Exp#5 and Exp#6)

A. Evaluation Methodology

Configuration. For the Alibaba dataset, recall that it spans from July 2017 to June 2018 (§III-A). By default, we set the training phase from July 2017 to April 2018 (10 months) and the testing phase for May 2018 (one month). RODMAN predicts disk failures in the testing phase. We set a high training-to-testing ratio to 10:1 by default, so as to have sufficient positive samples for training (as a reference, previous work sets the training-to-testing ratio to 4:1 [10] or 3:1 [28] for the Backblaze dataset evaluation); nevertheless, we also consider smaller training-to-testing ratios starting from 2:1 (Exp#6) and in the Backblaze dataset evaluation (see below). To mitigate data imbalance and the bias toward the substantial volume of negative samples, our training chooses the positive samples over the entire training phase, while choosing the negative samples only on the last day observed (i.e., the end of April 2018 without the observation window, or the last day before the observation window if enabled).

For the Backblaze dataset (§III-B), we change the training-to-testing ratio to 3:1 as in [28]. As in the Alibaba dataset evaluation, our training chooses the positive samples over the entire training phase and the negative samples only on the last day observed to mitigate data imbalance. Given the long dataset durations (18 months for H1 and 40 months for S1), we apply model training in a sliding fashion to allow multiple runs. Specifically, we use the first three months (e.g., January to March) as the training phase and the fourth month (i.e., April) as the testing phase. We slide one month (i.e., February to April for training and May for testing) for the next run, and so on. We have 15 and 37 runs in total for H1 and S1, respectively. We present the average results over all runs.

Metrics. Our disk failure prediction is a binary classification problem (i.e., failed or healthy). We focus on two metrics:

- **True positive rate (TPR):** The ratio of the number of predicted failed disks to the total number of actual disk failures in one-month testing.
- **False positive rate (FPR):** The ratio of the number of falsely predicted failed disks (which are indeed healthy) to the total number of healthy disks in one-month testing.

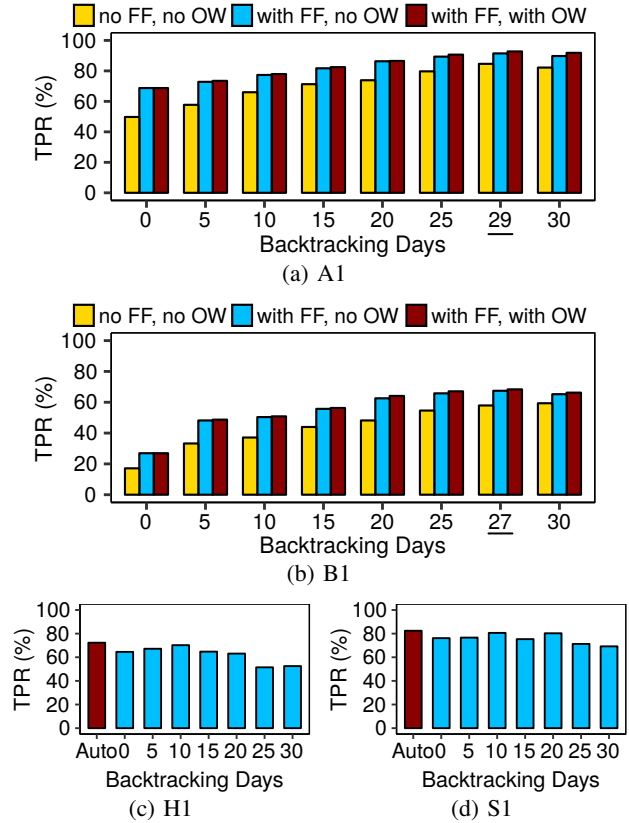


Figure 6: Exp#1 (Effectiveness of automated pre-failure backtracking). We show the TPRs of every five days (from 0 to 30 backtracking days) and the TPR of our automatically determined backtracking days (29 days for A1 and 27 days for B1 as underlined in the figures; “Auto” for H1 and S1). For A1 and B1, we compare two components: failure-type filtering (“FF”) and observation window (“OW”).

For the Alibaba dataset, we set the default FPR threshold to 0.1% as in Microsoft’s production [39]. We mainly present the results for disk models A1 and B1, while we address other disk models in the Alibaba dataset in §V-C. For the Backblaze dataset, we set a higher default FPR threshold to 4% to make the TPR comparable to that for the Alibaba dataset. Note that we still observe the accuracy gain of RODMAN for different FPR thresholds (Exp#5).

B. Analysis of Data Preprocessing Techniques

Exp#1 (Effectiveness of automated pre-failure backtracking). We first consider the Alibaba dataset. Recall that our automated pre-failure backtracking selects the backtracking window as 29 and 27 days for A1 and B1, respectively (§IV-C). We evaluate RODMAN for various lengths of backtracking windows and show the effectiveness of automated pre-failure backtracking. Before running the experiment, we have enabled spline-based data filling. We also compare two components of RODMAN: (i) failure-type filtering (i.e., using only the disk failures of predictable failure types for training instead of using all disk failures), and (ii) observation window (i.e., discarding a window of samples before the end of training for healthy disks).

Figures 6(a) and 6(b) show the TPR results versus the number of backtracking days for A1 and B1, respectively. First, the TPR increases as we increase the number of backtracking days from zero, as we now introduce more positive samples to alleviate data imbalance. Without pre-failure backtracking (the zero-day case), RODMAN can only correctly predict 68.7% of disk failures of A1 and 26.9% disk failures of B1 when both the failure-type filtering and the observation window are enabled. As we increase the number of backtracking days, the TPR for both disk models increases and reaches the highest between the 25 and 30 backtracking days (note that the TPR differences in this range are within 2% for both disk models). In particular, the TPR reaches 92.8% for A1 and 68.4% for B1 in our automatically determined backtracking days (29 and 27 days, respectively). After 30 backtracking days, the TPR decreases, as we may now falsely inject more positive samples. This shows that our automated pre-failure backtracking can reach the highest TPR range.

We next compare the TPR with and without failure-type filtering for A1 and B1. With failure-type filtering, the TPR increases for both disk models. For example, without pre-failure backtracking (the zero-day case), failure-type filtering itself increases the TPR from 49.8% to 68.7% for A1 and from 17.1% to 26.9% for B1. We provide more detailed evaluation of failure-type filtering in Exp#2.

We further study the TPR gains with the observation window (which equals the number of backtracking days (§IV-C)). Enabling the observation window for non-zero backtracking days on top of failure-type filtering further increases the TPR for both disk models in *all* cases, by 0.20-2.09% and 0.48-1.77% for A1 and B1, respectively. Although the accuracy improvement is small compared to the gains of failure-type filtering, we regard the observation window as a complementary approach for pre-failure backtracking: while pre-failure backtracking focuses on adding positive samples, the observation window keeps only the obvious negative samples and drops the ambiguous ones.

Finally, we validate our analysis with the Backblaze dataset. We study the accuracy gain when automated pre-failure backtracking with the observation window is enabled (recall that the Backblaze dataset has no failure types). Figures 6(c) and 6(d) show the TPR results versus the number of backtracking days for H1 and S1, respectively; we omit the plots for the backtracking days from 35 to 60 days as the TPR keeps decreasing. The automated backtracking days vary from 2 to 58 days for H1 and from 3 to 40 days for S1 across different runs. On average, automated pre-failure backtracking achieves the highest TPR, which is 72.3% for H1 and 82.4% for S1.

Exp#2 (Effectiveness of failure-type filtering). Recall that with failure-type filtering, we use the failures of predictable failure types (i.e., data corruptions, disk-not-found errors, and unhealthy disks for A1, and data corruptions for B1) for training. We now give a breakdown of the prediction accuracy of RODMAN for each failure type, with and without failure-type filtering. Here, we have enabled automated pre-failure backtracking with the observation window and spline-based

Type	A1		B1	
	w/o FF	w/ FF	w/o FF	w/ FF
Data corruptions	81.4%	95.1%	51.0%	70.2%
I/O request errors	88.5%	94.2%	56.8%	61.1%
Unhandled errors	92.0%	96.0%	60.6%	69.7%
Disk-not-found errors	92.3%	76.9%	50.0%	0%
Unhealthy disks	42.9%	71.4%	Nil	Nil
File system corruptions	Nil	Nil	Nil	Nil
Others	95.5%	90.9%	100.0%	100.0%

Table IX: Exp#2 (Effectiveness of failure-type filtering). We report the TPR for each failure type with or without failure-type filtering (“FF”); “Nil” means no failures belong to the failure type in testing.

data filling. We focus on A1 and B1 in the Alibaba dataset.

Table IX shows the TPR results for different failure types with and without failure-type filtering. We make two observations. First, RODMAN successfully identifies the failures of unpredictable failure types (e.g., unhandled errors), even being trained with only predictable failure types. Second, for most failure types, failure-type filtering improves the prediction accuracy. An exception is disk-not-found errors, which show a lower TPR for both disk models with failure-type filtering (another exception is “Others”), even though disk-not-found errors are a predictable failure type in A1.

One explanation to the above observations is that various disk failure symptoms can share the same root causes (e.g., both data corruptions and I/O request errors can be caused by a failing disk sector) [18]. Thus, training a classifier with only representative failure types can correctly identify different types of imminent disk failures, including those of unpredictable failure types. The trade-off is that by filtering the unpredictable failure types, we may unexpectedly drop disk failures whose root causes manifest as both predictable and unpredictable failure types. Nevertheless, the overall prediction accuracy improves, as shown in Exp#1.

Exp#3 (Effectiveness of spline-based data filling). We evaluate different data filling approaches, including forward filling, linear interpolation, and cubic spline interpolation. Note that the data filling approaches fill in different values, and hence return different backtracking windows from our automated pre-failure backtracking. For example, for the Alibaba dataset, the backtracking windows for forward filling, linear interpolation, and cubic spline interpolation are chosen as 26, 28, and 29 days, respectively for A1, as well as 24, 27, and 27 days, respectively, for B1. We also evaluate the no-filling case by training the raw dataset directly, in which we set the backtracking windows as 29 and 27 days for A1 and B1, respectively, as in cubic spline interpolation. Here, we have enabled failure-type filtering for A1 and B1.

Figure 7 shows the results. For the Alibaba dataset, no-filling has a lower TPR than both forward filling and cubic spline interpolation, implying that data filling is necessary for high prediction accuracy. Also, cubic spline interpolation achieves the highest TPR (92.8% for A1 and 68.4% for B1). A surprising observation is that linear interpolation has the lowest TPR (even lower than no-filling). One possible reason is that most failure-related attributes series are of non-linear patterns

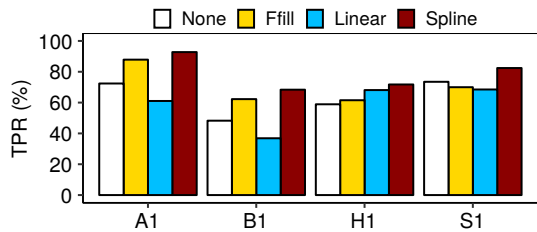


Figure 7: Exp#3 (Effectiveness of spline-based data filling). We compare no-filling (“None”), forward filling (“Ffill”), linear interpolation (“Linear”), and cubic spline interpolation (“Spline”).

(e.g., SM5, SM187, and SM197). For non-linear patterns, both forward filling and linear interpolation fill in less accurate values compared to cubic spline interpolation; even worse, linear interpolation may introduce more noise samples than forward filling, as the latter only fills any missing gap with duplicate but non-noise samples.

For the Backblaze dataset, cubic spline interpolation still achieves the highest TPR (72.3% for H1 and 82.4% for S1). Note that the rankings of prediction accuracy across different filling methods are different in the Alibaba and Backblaze datasets. One possible reason is that the two datasets have different data missing rates and patterns (Table IV vs. Table V).

C. Analysis of Whole RODMAN

We evaluate RODMAN as a whole with all data preprocessing techniques enabled (i.e., failure-type filtering (for the Alibaba dataset only), spline-based data filling, and automated pre-failure backtracking with the observation window). We compare RODMAN with the *baseline*, in which we only perform data filling with cubic spline interpolation on the raw dataset but do not apply other data preprocessing techniques.

Exp#4 (Comparisons with state-of-the-arts). We compare the accuracy of RODMAN with two state-of-the-art ML-based disk failure prediction approaches [10], [28]. The ML model in [10] is Regularized Greedy Forests (RGF) [33], while that in [28] is Random Forests (RF) [11]. Our goal here is not to advocate any particular ML model; instead, we show that RODMAN improves the respective accuracy of a given ML model as a general framework compared to the baseline.

One challenge is that both approaches in [10], [28] build on completely different datasets, so it is infeasible to completely reproduce their methodologies. Thus, we make the “best efforts” to implement their approaches based on their description and conduct our comparison study under fair conditions. Specifically, we train and test all approaches using our datasets. Since the feature construction process largely depends on the data preprocessing and statistical analysis of the specific datasets, for fair comparisons, we choose our constructed features for all approaches.

To this end, we compare the baseline and RODMAN on three ML models: LightGBM, RGF, and RF (i.e., six variants in total). We implement the baseline RGF and RF to resemble the approaches in [10] and [28], respectively. To alleviate data imbalance, we perform the standard under-sampling technique

ML models		A1	B1	H1	S1
LightGBM	Baseline	69.7%	57.1%	64.6% (±21.3%)	76.2% (±4.4%)
	RODMAN	92.8%	68.4%	72.3% (±15.3%)	82.4% (±3.6%)
RGF	Baseline	67.2%	53.4%	56.4% (±20.6%)	65.0% (±8.1%)
	RODMAN	88.6%	67.2%	62.6% (±17.3%)	75.4% (±5.0%)
RF	Baseline	62.6%	48.3%	50.7% (±19.7%)	73.5% (±3.4%)
	RODMAN	86.4%	64.5%	60.7% (±17.6%)	80.9% (±3.5%)

Table X: Exp#4 (Comparison with state-of-the-arts). For H1 and S1, we also report 95% confidence intervals (in brackets) of all runs.

on negative samples as described in [10], [28], such that the ratio of positive to negative samples is 1:10 (the prediction accuracy is maintained for various ratios from 1:1 to 1:10 [28]). In contrast, for the Alibaba (Backblaze) dataset, RODMAN and its baseline implementation use the positive samples in the whole 10-month (3-month) training phase and the negative samples on the last day observed (§V-A). Furthermore, we conduct grid-search and configure the following model settings that achieve high prediction accuracy: for LightGBM, we set 2,000 trees; for RGF, we set the maximum number of trees as 2,000 and use L2-norm regularization for RGF; for RF, we set 2,000 trees.

Table X shows the results. RODMAN increases the TPR of all ML models over the baseline by 21.4-23.7%, 11.3-15.8%, 6.2-10.0%, and 6.2-10.4% for A1, B1, H1, and S1, respectively. This shows that RODMAN improves the prediction accuracy for different ML models and different datasets.

Exp#5 (Impact of FPR thresholds). In general ML-based prediction, we can increase the TPR by increasing the FPR threshold (or vice versa). Here, we vary different FPR thresholds and measure the corresponding TPR results to verify whether the prediction accuracy gain of RODMAN over the baseline (without RODMAN) is still preserved in both Alibaba and Backblaze datasets. Figures 8(a) and 8(b) show the TPR results of A1 and B1, respectively, when we vary the FPR threshold from 0.04% to 0.1%, while Figures 8(c) and 8(d) show the TPR results of H1 and S1, respectively, when we vary the FPR threshold from 1.0% to 4.0%. The TPR gain of RODMAN over the baseline is fairly stable for different FPR thresholds, with around 20%, 10%, 8%, and 6% gains for A1, B1, H1, and S1 respectively.

Exp#6 (Impact of training periods). Recall that for the Alibaba dataset, we use a 10-month training period by default. We now reduce the length of the training period for positive samples. Clearly, reducing the length of the training period reduces the TPR, yet our goal here is to evaluate the robustness of RODMAN to the prediction accuracy gain over the baseline (recall that we still choose one day of negative samples (§V-A)). We vary the training period from 2 to 10 months, counted backwards from April 2018, while we still set the test phase in May 2018. Figure 9 shows the impact of different training periods. If we reduce the training period for positive samples

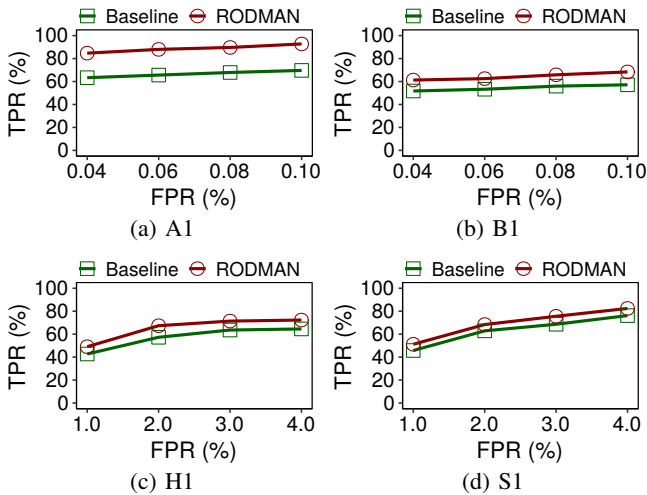


Figure 8: Exp#5 (Impact of FPR thresholds).

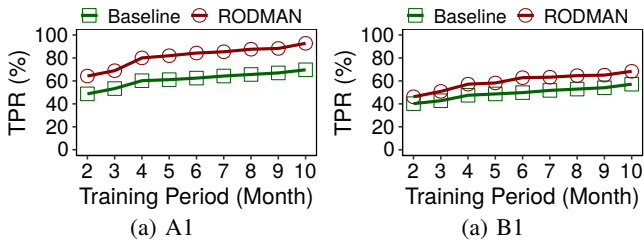


Figure 9: Exp#6 (Impact of training periods).

from the default 10 months to 2 months, the TPR of RODMAN drops from 92.8% to 64.3% for A1 and from 68.4% to 46.2% for B1, since we now have fewer positive samples for training. Similar to Exp#5, RODMAN consistently increases the TPR over the baseline by around 20% and 10% for A1 and B1, respectively, for different training periods.

Remarks. We show that RODMAN improves the prediction accuracy via its data preprocessing techniques, and its accuracy gain is shown in both Alibaba and Backblaze datasets, different ML models, as well as different parameter choices. For the Alibaba dataset, we also validate the effectiveness of RODMAN for other disk models. Here, we choose the disk models A2 and B2, since both of them also have large numbers of disks, as well as large numbers of positive samples for training. The TPR of RODMAN achieves 96.4% and 63.2% for A2 and B2, respectively, while that of the baseline only achieves 70.6% and 43.9%, respectively (we do not illustrate the results in plots here). We do not validate RODMAN for other disk models (e.g., for vendors ‘C’, ‘D’, and ‘E’), as we do not have sufficient positive samples for training and our prediction analysis becomes less representative. We pose the analysis for such disk models in future work.

VI. RELATED WORK

Field measurements. Extensive field measurement studies show the prevalence of disk failures in production environments. Earlier studies [32], [35] show that the actual disk failure

rates are much higher than the datasheet values. In particular, Google’s study [32] shows that over half of failed disks do not record any SMART failure signal. In addition to disk failures, faulty interconnects and protocol stack errors are also dominant [21]. Furthermore, field studies on NetApp clusters reveal patterns of latent sector errors [9], [34] and silent data corruptions [8]. A more recent study from EMC [27] analyzes the failures of about one million of disks over a five-year span, and shows that reallocation sector counts are good indicators of predicting disk failures. Instead of emphasizing the prevalence of disk failures, our field study focuses on motivating the need of data preprocessing. To address the limitations of SMART logs alone [32], we leverage syslogs and trouble tickets for more accurate characterization of disk failures.

Disk failure prediction. A spate of studies show that highly accurate disk failure prediction is achievable using classical statistical techniques and machine learning models. Examples include Bayesian classifiers [19], rank-sum tests [20], Markov models [14], [40], rule-based learning [6], back-propagation neural networks [42] and recurrent neural networks [24], regularized greedy forests [10], random forests [28], and online random forests [38]. Based on disk failure prediction, some studies further propose proactive fault tolerance approaches to protect against soon-to-fail disks, such as proactive replication [26] and adaptive scrubbing [28]. However, existing studies mainly validate their proposals using the datasets from a small-scale disk population (e.g., [6], [14], [19], [20], [24]–[26], [40], [42]) or the public Backblaze SMART logs [3] (e.g., [10], [28], [38]). We complement these studies through our proposed data preprocessing techniques and the correlation of multiple data sources (i.e., SMART logs, syslogs, and trouble tickets).

VII. CONCLUSION

We have witnessed extensive ML-based disk failure prediction studies in the literature, but limited emphasis is put on proper preprocessing on training datasets. This paper fills the void and posits the need for improving the quality of the training datasets used for ML model training instead of designing new ML models. We present RODMAN, a robust disk failure prediction management pipeline that is now deployed in a large-scale cloud service provider. It builds on three data preprocessing techniques (i.e., failure-type filtering, spline-based data filling, and automated pre-failure backtracking) to carefully refine and correlate SMART logs, syslogs, and trouble tickets before feeding them into any ML model. We show that RODMAN improves the disk failure prediction accuracy for general ML models on different datasets.

REFERENCES

- [1] Amazon’s Cloud. <https://www.bloomberg.com/news/2014-11-14/5-numbers-that-illustrate-the-mind-bending-size-of-amazon-s-cloud.html>.
- [2] Apache Hive. <https://hive.apache.org/>.
- [3] Backblaze published datasets. <https://www.backblaze.com/b2/hard-drive-test-data.html>.
- [4] LightGBM Repository. <https://github.com/microsoft/LightGBM>.
- [5] MaxCompute. <https://www.alibabacloud.com/product/maxcompute>.

- [6] V. Agarwal, C. Bhattacharyya, T. Niranjana, and S. Susarla. Discovering rules from disk events for predicting hard drive failures. In *Proc. of IEEE ICMLA*, 2009.
- [7] R. Alagappan, A. Ganesan, Y. Patel, A. C. Arpaci-Dusseau, and R. H. Arpaci-Dusseau. Correlated crash vulnerabilities. In *Proc. of USENIX OSDI*, 2016.
- [8] L. N. Bairavasundaram, A. C. Arpaci-Dusseau, R. H. Arpaci-Dusseau, G. R. Goodson, and B. Schroeder. An analysis of data corruption in the storage stack. *ACM Trans. on Storage*, 4(3):8, Nov 2008.
- [9] L. N. Bairavasundaram, G. R. Goodson, S. Pasupathy, and J. Schindler. An analysis of latent sector errors in disk drives. In *Proc. of ACM SIGMETRICS*, 2007.
- [10] M. Botezatu, I. Giurgiu, J. Bogojeska, and D. Wiesmann. Predicting disk replacement towards reliable data centers. In *Proc. of ACM SIGKDD*, 2016.
- [11] L. Breiman. *Random Forests*. 2001.
- [12] R. Caruana, N. Karampatziakis, and A. Yessenalina. An empirical evaluation of supervised learning in high dimensions. In *Proc. of ACM ICML*, pages 96–103, 2008.
- [13] R. Caruana and A. Niculescu-Mizil. An empirical comparison of supervised learning algorithms. In *Proc. of ACM ICML*, pages 161–168, 2006.
- [14] B. Eckart, X. Chen, X. He, and S. L. Scott. Failure prediction models for proactive fault tolerance within storage systems. In *Proc. of IEEE MASCOTS*, 2009.
- [15] P. Fearnhead. *Exact and Efficient Bayesian Inference for Multiple Changepoint Problems*. 2006.
- [16] R. Gerhards. The syslog protocol. <https://tools.ietf.org/html/rfc5424>, Mar 2009. RFC 5424.
- [17] H. S. Gunawi, M. Hao, R. O. Suminto, A. Laksono, A. D. Satria, J. Adityatama, and K. J. Eliazar. Why does the cloud stop computing? lessons from hundreds of service outages. In *Proc. of ACM SOCC*, 2016.
- [18] H. S. Gunawi, R. O. Suminto, R. Sears, C. Gollhofer, S. Sundararaman, X. Lin, T. Emami, W. Sheng, N. Bidokhti, C. McCaffrey, G. Grider, P. M. Fields, K. Harms, R. B. Ross, A. Jacobson, R. Ricci, K. Webb, P. Alvaro, H. B. Runesha, M. Hao, and H. Li. Fail-slow at scale: Evidence of hardware performance faults in large production systems. In *Proc. of USENIX FAST*, 2018.
- [19] G. Hamerly and C. Elkan. Bayesian approaches to failure prediction for disk drives. In *Proc. of ACM ICML*, 2001.
- [20] G. F. Hughes, J. F. Murray, K. Kreuz-Delgado, and C. Elkan. Improved disk-drive failure warnings. *IEEE Trans. on Reliability*, 51(3):350–357, 2002.
- [21] W. Jiang, C. Hu, Y. Zhou, A. Kanevsky, and N. Appliance. Are Disks the Dominant Contributor for Storage failures. In *Proc. of USENIX FAST*, 2008.
- [22] E. Jones, T. Oliphant, P. Peterson, et al. SciPy: Open source scientific tools for Python. <http://www.scipy.org/>.
- [23] G. Ke, Q. Meng, T. Finley, T. Wang, W. Ma, Q. Ye, and T.-Y. Liu. LightGBM: A highly efficient gradient boosting decision tree. In *Proc. of NIPS*, 2017.
- [24] J. Li, X. Ji, Y. Jia, B. Zhu, G. Wang, Z. Li, and X. Liu. Hard drive failure prediction using classification and regression trees. In *Proc. of IEEE/IFIP DSN*, 2014.
- [25] J. Li, R. J. Stones, G. Wang, Z. Li, X. Liu, and K. Xiao. Being accurate is not enough: New metrics for disk failure prediction. In *Proc. of IEEE SRDS*, 2016.
- [26] P. Li, J. Li, R. J. Stones, G. Wang, Z. Li, and X. Liu. Procode: A proactive erasure coding scheme for cloud storage systems. In *Proc. of IEEE SRDS*, 2016.
- [27] A. Ma, F. Douglis, G. Lu, D. Sawyer, S. Chandra, and W. Hsu. RAIDShield: Characterizing, monitoring, and proactively protecting against disk failures. In *Proc. of USENIX FAST*, 2015.
- [28] F. Mahdisoltani, I. Stefanovici, and B. Schroeder. Proactive error prediction to improve storage system reliability. In *Proc. of USENIX ATC*, 2017.
- [29] F. J. Massey. The Kolmogorov-Smirnov test for goodness of fit. *Journal of the American Statistical Association*, 46(253):68–78, 1951.
- [30] T. Oliphant. *Guide to NumPy*. 2006.
- [31] F. Pedregosa, G. Varoquaux, A. Gramfort, V. Michel, B. Thirion, O. Grisel, M. Blondel, P. Prettenhofer, R. Weiss, V. Dubourg, J. Vanderplas, A. Passos, D. Cournapeau, M. Brucher, M. Perrot, and E. Duchesnay. Scikit-learn: Machine learning in Python. *Journal of Machine Learning Research*, 12:2825–2830, 2011.
- [32] E. Pinheiro, W.-D. Weber, and L. A. Barroso. Failure trends in a large disk drive population. In *Proc. of USENIX FAST*, 2007.
- [33] J. Rie. Learning nonlinear functions using regularized greedy forest. *IEEE Trans. on Pattern Analysis and Machine Intelligence*, 36(5):942–954, 2014.
- [34] B. Schroeder, S. Damouras, and P. Gill. Understanding latent sector errors and how to protect against them. In *Proc. of USENIX FAST*, 2010.
- [35] B. Schroeder and G. A. Gibson. Disk failures in the real world: What does an MTTF of 1,000,000 hours mean to you? In *Proc. of USENIX FAST*, 2007.
- [36] C. Spearman. The proof and measurement of association between two things. *The American Journal of Psychology*, 100(3/4):441–471, 1987.
- [37] J. Stoer and R. Bulirsch. *Introduction to numerical analysis*, volume 12. Springer-Verlag New York, 3 edition, 2002.
- [38] J. Xiao, Z. Xiong, S. Wu, Y. Yi, H. Jin, and K. Hu. Disk failure prediction in data centers via online learning. In *Proc. of ICPP*, 2018.
- [39] Y. Xu, K. Sui, R. Yao, H. Zhang, Q. Lin, Y. Dang, P. Li, K. Jiang, W. Zhang, J.-G. Lou, M. Chintalapati, and D. Zhang. Improving service availability of cloud systems by predicting disk error. In *Proc. of USENIX ATC*, 2018.
- [40] Z. Ying, L. Xiang, S. Gan, and W. Zheng. Predicting disk failures with HMM- and HSMM-based approaches. In *Proc. of IEEE ICDM*, 2010.
- [41] M. Zheng, J. Tucek, F. Qin, and M. Lillibridge. Understanding the robustness of SSDs under power fault. In *Proc. of USENIX FAST*, 2013.
- [42] B. Zhu, G. Wang, X. Liu, D. Hu, S. Lin, and J. Ma. Proactive drive failure prediction for large scale storage systems. In *Proc. of IEEE MSST*, 2013.